Pergamon

Bioorganic & Medicinal Chemistry, Vol. 5, No. 5, pp 843–856, 1997

PII: S0968-0896(97)00023-0
0968-0896/97 $17.00 + 0.00

2-D and 3-D Modeling of Imidazoline Receptor Ligands: Insights into Pharmacophore

A. Carrieri,[a] L. Brasili,[b] F. Leonetti,[a] M. Pigini,[c] M. Giannella,[c] P. Bousquet[d] and A. Carotti[a,*]

[a]*Dipartimento Farmaco-Chimico, Università degli Studi di Bari, Via Orabona 4, 70126-Bari, Italy*
[b]*Dipartimento di Scienze Farmaceutiche, Università di Modena, Italy*
[c]*Dipartimento di Scienze Chimiche, Università di Camerino, Italy*
[d]*Laboratoire de Pharmacologie Cardiovasculaire et Renale, Université Louis Pasteur, Strasbourg, France*

Abstract—A 3-D quantitative structure–activity relationship (3-D QSAR) study was carried out using comparative molecular field analysis (CoMFA) on both imidazoline (I_2R) and α_2 receptor binding affinities of a large series of 2-substituted imidazolines. Significant cross-validated correlations, having promising predictive ability, were obtained along with 3-D pharmacophore models that defined the spatial regions where steric and electrostatic interactions may modulate the in vitro binding affinities and indicated possible physicochemical and structural requirements for I_2/α_2 receptor selectivity. © 1997 Elsevier Science Ltd.

Introduction

Comparative molecular field analysis (CoMFA)[1] is a promising tool for studying quantitative structure–activity (property) relationships (QSAR, QSPR).[2] Unlike the traditional Hansch analysis, which makes use of substituent parameters, CoMFA tries to correlate the biological activity (target property) of a series of molecules (not necessarily congeneric) with their steric and electrostatic fields sampled at grid points defining a large 3-D box (region) around the molecule. CoMFA columns (descriptors) are constituted by the steric (Lennard–Jones) and electrostatic (Coulomb) potentials computed for each molecule, at each grid point, by means of a suitable probe, usually, an sp^3 carbon atom with a charge of +1. Partial least squares (PLS)[3] is used as the regression method to develop the relationship between independent variables (steric and electrostatic potentials) and biological activity (dependent variable). PLS analysis produces model equations that explain the variance in the target property in terms of the independent variables.[4] The optimum number of components (latent variables) is determined by cross-validation and the model predictive ability is assessed by cross-validated $r^2(r^2_{cv}, q^2)$.[5]

The graphical representation of CoMFA results (isocontour maps) indicated the regions where the variations in steric and electrostatic properties of different molecules in a data set are correlated with the variation of biological activity. Even though much care has to be used to avoid an overinterpretation of the contour maps in the definition of the binding site topology (receptor mapping) no doubt the CoMFA graphs may be taken as useful indications to guide future synthesis and to develop sound hypotheses on the nature of putative ligand–receptor interactions.

Here we present a study that employs CoMFA methodology to rationalize the relationship between the structural and physicochemical features of a series of 2-substituted imidazolines and their binding affinities both to I_2 and α_2 receptors.[6]

While several studies have dealt with direct[7,8] and indirect modeling[9] of α_2-adrenoceptor, to the best of our knowledge, the present report is the first attempt to unravel structure–affinity relationships for imidazoline receptor (I_2R) ligands. In the absence of any 3-D structural data on I_2R, we have used indirect methods to model both I_2 and α_2 receptor affinity data reported in Table 1. Only in this way is a direct comparison of the results from the two separated SAR studies possible and this may give insight into the key structural requirements for receptor selectivity.

I_2R binding affinities

In a preliminary step we analyzed a small set of congeneric I_2R ligands, namely the *ortho*-substituted phenoxy derivatives (OPS) **1–4**, **6–8**, **10**, **12**, **13**, **15** and **16** using for data analysis a cross-validated multilinear regression technique according to the Hansch approach (2-D QSAR).[10,11] In the authors' opinion, the Hansch analysis, when dealing with congeneric series, is still the method that yields the most valuable indications for a physicochemical interpretation of the SAR. Moreover, results from 2-D QSAR are often complementary to those obtained by 3-D QSAR methods allowing a synergic interpretation of complex (bio)chemical pro-

Table 1. I_2 and α_2 receptor binding affinities[a] of 2-substituted imidazolines **1–40**

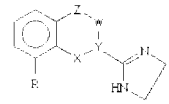

Compds[b]	R	X	Y	W	Z	ΔE K_{cal}/mol[c]	pK_i IR	pK_i α_2	Selectivity[d]
1	CH_2–CH=CH_2	O	CH_2	–	–	5.53	8.85 (8.76)		
						nd	[8.95]		
2	CH_2–C_6H_5	O	CH_2	–	–	7.52	6.70 (7.14)	6.52	0.18
						(2.39)	[6.19]	(6.50)	
3	cC_3H_5	O	CH_2	–	–	5.32	8.41 (8.09)	7.77	0.64
						(3.69)	[8.44]	(7.88)	
4	$CH(CH_3)_2$	O	CH_2	–	–	3.31	8.66 (7.86)	6.59	2.07
						(0.25)	[8.37]	(6.70)	
5	$CH(CH_3)_2$	O	$CH(CH_3)$	–	–	6.71	5.29 (5.49)		
						(2.38)	[5.88]		
6	CH_2CH_3	O	CH_2	–	–	5.11	8.57 (8.64)		
						(0.84)	[8.53]		
7	$CH_2CH_2CH_3$	O	CH_2	–	–	5.90	8.21 (8.41)		
						(3.84)	[8.47]		
8	CH_3	O	CH_2	–	–	3.45	9.05 (8.80)		
						(0.22)	[8.77]		
9	CH_3	O	$CH(CH_3)$	–	–	7.89	6.70 (6.40)		
						(2.39)	[6.31]		
10	$OCH(CH_3)_2$	O	CH_2	–	–	6.82	7.07 (7.44)		
						(0.30)	[7.14]		
11	$OCH(CH_3)_2$	O	$CH(CH_3)$	–	–	8.10	5.62 (4.87)		
						(3.14)	[5.12]		
12	C_6H_5	O	CH_2	–	–	6.78	6.52 (6.46)	7.10	−0.58
						nd	[6.36]	(7.09)	
13	H	O	CH_2	–	–	2.70	9.04 (8.46)	7.28	1.76
						(0.19)	[8.61]	(7.41)	
14	H	O	$CH(CH_3)$	–	–	6.79	5.57 (6.07)	7.01	−0.31
						(2.78)	[6.14]	(7.05)	
15	$CH(CH_3)CH_2CH_3$	O	CH_2	–	–	7.68	7.30 (7.50)		
						(5.72)	[7.59]		
16	$C(CH_3)_3$	O	CH_2	–	–	2.97	6.70 (7.22)		
						(2.13)	[7.39]		
17	H	CH_2	CH_2	–	–	2.22	8.60	5.70	2.90
						(1.55)	(8.21)	(5.51)	
18	H	S	CH_2	–	–	3.31	7.31	6.70	0.61
						(1.49)	(8.01)	(6.79)	
19	H	NH	CH_2	–	–	4.88	7.48		
						nd	(8.19)		
20	H	CH=CH trans		–	–	0.97	8.72	4.85	3.87
						nd	(8.48)	(5.11)	
21	H	CH=C(CH_3) trans		–	–	2.54	7.96		
						nd	(7.81)		
22	H	CHC_6H_5	CH_2	–	–	6.81	5.54	6.15	−0.61
						(2.15)	(5.46)	(6.25)	
23	H	O	CH	CH_2	O	1.76	8.37	7.72	0.65
						(1.27)	(7.95)	(7.68)	
24	H	CH_2	CH	CH_2	O	1.37	7.80	6.87	0.93
						(0.59)	(8.31)	(7.07)	
25	H	CH=C		CH_2	O	1.30	8.43	6.15	2.28
						nd	(8.17)	(5.80)	
26	H	CH=C		CH_2	CH_2	1.21	7.95		
						nd	(8.55)		
27	H	O	CH	CH_2	S	2.19	7.31	8.35	0.22
						(1.13)	(8.01)	(8.07)	
28	H	C=O	C=CH		O	0.34	5.68		
						nd	(5.87)		

Table 1. Continued

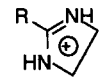

Compds[b]	R	ΔE K_{cal}/mol[c]	pK_i IR	pK_i α_2	Selectivity[d]
29	1′-Naphthyl	0.93	7.66	5.38	2.28
		nd	(7.80)	(5.17)	
30	2′-Naphthyl	0.00	9.07	4.80	4.27
		nd	(8.45)	(5.06)	
31	9′-Anthryl	2.79	6.00	5.26	0.74
		nd	(6.15)	(5.52)	
32	9′-Phenanthryl	1.42	7.15	5.52	1.63
		nd	(6.77)	(5.54)	
33	3′-Biphenyl	2.80	7.62	5.21	2.41
		nd	(7.67)	(5.09)	
34	1′-Naphthylmethyl	5.44	7.00	8.56	−1.56
		(3.85)	(7.25)	(8.38)	
35	2′-Naphthylmethyl	5.50	6.52	7.03	−0.51
		(4.20)	(6.49)	(6.94)	
36	1′-Naphthoxymethyl	4.22	8.72	7.17	1.55
		(0.47)	(8.85)	(7.23)	
37	2′-Naphthoxymethyl	3.64	8.41	5.96	2.45
		(0.52)	(8.13)	(5.65)	
38	2′-Naphthoxyethyl	5.82	5.44	5.39	0.05
		(2.74)	(5.68)	(5.29)	
39	CH2-C6H5	1.51	6.70	6.70	0.00
		(0.22)	(6.72)	(7.22)	
40	2′,5′-Dichloroanilino	4.24	6.10	8.30	−2.20
		nd	(5.86)	(7.75)	

[a]Reported as pK_i. The predicted pK_i values from noncross-validated model equations CI3a (I_2) and CA3a (α_2) are reported in parentheses. The predicted pK_i values coming from noncross-validated equation CO3a and referring to the OPS subset, are indicated in square brackets.
[b]Common names: **3**, Cirazoline; **23**, Idazoxan; **34**, Naphazoline; **39**, Tolazoline; **40**, Clonidine. Proposed names:[6] **20**, Tracizoline; **30**, Benazoline.
[c]Relative to the CI3a model of the imidazoline receptor ligands. ΔE represents the energy differences among the selected conformers for CoMFA and the minimum energy conformers calculated with AM1 (upper values) and the *solvent continuum* method (MacroModel, in brackets. nd: not determined due to low quality parametrization in the AMBER* Force Field of MacroModel.
[d]Selectivity expressed as pK_i (I_2) − pK_i (α_2).

cesses as recently shown in the study of the enzyme inhibition[12–14] and the chromatographic enantioseparation on chiral stationary phases.[15,16]

Since the OPS series was designed to explore the *ortho* region mostly in terms of steric accessibility, only physicochemical and geometric parameters describing such a property have been taken into account as substituent descriptors (see Experimental).

The most significant one-variable equation was as follows:

$$pK_i = -1.07(\pm 0.45)MR + 9.60(\pm 0.78) \quad (1)$$

$$n = 12,\ q^2 = 0.635,\ r^2 = 0.738,\ s = 0.530$$

where K_i is the inhibition constant, MR is the molar refractivity, n is the number of data points, q is the cross-validated correlation coefficient, r is the correlation coefficient, and s is the standard deviation from regression. In parentheses the 95% confidence intervals are indicated.

Equation (1) suggests a limited receptor accessibility in the *ortho* space, with the most active compounds being those bearing small-sized substituents. Due to the dual nature of MR, which by definition is a measure of bulkiness and polarizability,[17] equation (1) might be indicative of interactions more complex than the steric ones, as already observed in similar studies of enzyme–ligand binding.[18]

The inclusion into equation 1 of further OPS congeners **5**, **9**, **11** and **14** having a C-methyl substituent on the oxymethylene bridge was possible only by means of the indicator variable I, which takes the value of 1 or 0, in the presence or absence of the methyl substituent, respectively. The following equation was formulated:

$$pK_i = -0.92(\pm 0.44)MR - 2.67(\pm 0.78)I + 9.36(\pm 0.77) \quad (2)$$

$$n = 16,\ q^2 = 0.716,\ r^2 = 0.821,\ s = 0.592$$

Equation (2) expresses in quantitative terms some already-evident activity profile of the OPS congeners.

In particular the dramatic drop of affinity caused by the introduction of the methyl substituents on the oxymethylene bridge is clearly pointed out. Even though equations (1) and (2) are particularly useful for a preliminary interpretation of the structure–activity relationships of the OPS-type congeners, a better characterization of the stereoelectronic requirements of the *ortho* as well as the *meta* and *para* regions is needed for a more complete study.

An extension of 2-D QSAR study to the whole set of I_2R ligands (40 compounds) was not possible due to the lack of congenericity and therefore to the difficulty of correctly parameterizing the structural and physicochemical features of the varying molecules. The biological data of I_2R ligands reported in Table 1 were then subjected to a 3-D QSAR study by CoMFA. A preliminary data analysis showed a good spread and distribution (Fig. 1) of the pK_i values, which spanned about a 4 log unit range (from 5.29 to 9.07); this was a good prerequisite for the derivation of meaningful models.

Molecular models and structure alignment for CoMFA

Molecular models of the compounds under study were constructed using the fragment library of the SYBYL 6.2 software. X-ray data from the crystallographic structural database were used as starting geometry for idazoxan[19] and clonidine.[20]

Even though the imidazoline ring should exist only in its protonated form at physiological pH, both neutral and charged molecules were taken into account and used in the derivation of the CoMFA models. The atomic charges used in CoMFA were from the AM1 calculations.

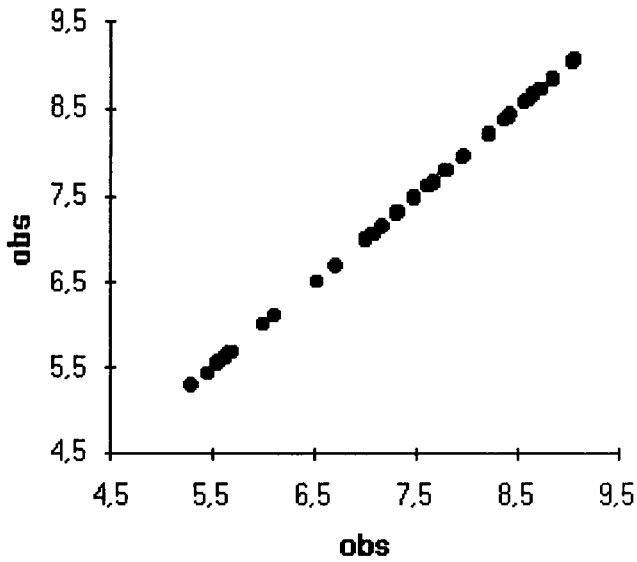

Figure 1. pK_i data distribution of I_2R ligands **1–40**.

Conformational analysis was performed by a systematic search of the torsional space. The pucker of the ring in compounds **23–27** was selected according to the X-ray data of (*S*)-idazoxan.

CoMFA results are strongly dependent on the criteria chosen for molecular superimposition (alignment rules) and therefore this determinant CoMFA step[21] was thoroughly explored.

Two different strategies of molecular alignment have been generally employed in CoMFA studies: one which is based on the strict selection of minimum energy conformers, and the second that seeks maximum overlap between conformers comprised within a relatively wide range of energy window. In both cases, model autoconsistency and higher predictive power are strongly pursued.

Since there is no definitive evidence to support one strategy over the other, we decided to use both in our analyses and to retain the alignments leading to the best models in terms of predictive ability. For the molecular overlap, besides an energy criteria in the selection of different conformers, we also used diverse fitting procedures and pharmacophoric elements (see below). This was done to give a different importance (weight) to the selected pharmacophoric features.

In a very preliminary modeling of the I_2R binding affinities,[22] we assigned to the five heavy atoms of the charged imidazoline ring a triple weight with respect to other pharmacophoric elements (aromatic ring centroids, heavy atoms in the flexible bridge, etc.) on the hypothesis that the electrostatic forces could play a dominant role in the binding to I_2R, compared to other possible physicochemical interactions.

However, to avoid an arbitrarily unbalanced fitting, we have analyzed here two diverse molecular superimpositions based on an equal weight of all the pharmacophoric elements. 2-(2-naphthyl) imidazoline **30** was chosen as the template because of its high affinity and relatively low conformational mobility. The minimum energy conformer having an interring dihedral angle $\phi = -32.3°$ was selected from a systematic conformational analysis and used as the template for the molecular overlay of charged and neutral molecules.

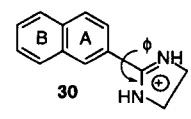

Each I_2R ligand molecule was subjected to a conformational analysis through a systematic search and all the conformers with an energy up to 8 kcal/mol above the global minimum were superposed onto the template. Whatever alignment criteria were used (see below) when only minimum energy conformers were considered, no significant models were obtained both for charged and neutral molecules. We therefore directed our efforts to the detection of those conformers that, on

Table 2. Statistical results of CoMFA analysis of OPS ligands **1–16**[a]

Alignment	q^2	ONC	n	r^2	s	F	Field(s)
CO1a	0.629	3	16	0.908	0.443	39.35	ste
CO2a	−0.818	3	16				ele
CO3a	0.481	5	16				ste + ele
CO4b	0.594	3	16	0.937	0.366	59.48	ste
CO5b	−1.039	3	16				ele
CO6b	0.267	2	16				ste + ele
NO1a	0.571	3	16	0.909	0.440	39.38	ste
NO2a	−0.322	1	16				ele
NO3a	0.221	2	16				ste + ele
NO4b	0.615	3	16	0.913	0.429	42.20	ste
NO5b	−0.105	1	16				ele
NO6b	0.268	2	16				ste + ele

[a]CO, NO: charged and neutral OPS ligands, respectively; a and b: different alignment criteria (see text); q: cross-validated correlation coefficient; **ONC**: optimal number of components used for the final analysis; n, r, s, and **F**: number of data points, correlation coefficient, standard deviation, and F statistics, respectively, for the noncross-validated final models; **Field**: CoMFA steric (ste) and electrostatic (ele) fields.

fitting onto the template, gave the lowest RMS values. Also in this case, no statistically significant models were derived. To reach a better overall molecular superposition, some torsion angles, in particular those of the ortho-substituents in the OPS series and of the flexible chain linking the imidazoline moiety, were therefore slightly adjusted, allowing an energy penalty above the global minimum, occasionally up to about 8 kcal/mol.

At a first impression, this value may seem unacceptably high but according to very recent findings[23] this is not the case, since for flexible molecules energy values well above the global minimum (up to 46 kcal/mol!) have been found for bound conformations of inhibitors in several X-ray-determined 3-D structures of inhibitor–protein complexes. Even though strain energy due to crystal packing forces may contribute to such a high energy content, those findings do suggest that ligands often bind to their macromolecular counterpart in high energy conformations.

However, to better analyze the apparently high energy content of some conformers selected for CoMFA, a conformational analysis was performed also by the *solvent continuum* method implemented in MacroModel v. 5.0. By this method it is possible to simulate the solvent effects on the conformation either in apolar (chloroform) or polar (water) medium. We have limited our analysis to the latter and to 26 compounds, in the protonated form, for which reliable force field parameters (AMBER*)[37] were available in MacroModel. For compounds having up to three rotatable bonds a systematic search (MULTIC algorithm, 30° step size, conjugate gradient minimizer, convergence criteria RMS<0.05 Å/kcal mol^2) was used whereas for compounds with more than three rotatable bonds the Monte Carlo method, sampling up to 3000 conformers for each analysis, was employed. The AM1 minimum energy conformers and the conformers selected for the previous CoMFA were imported in MacroModel and re-optimized in water medium without changing the torsion angles. A comparison of the energy differences resulting from AM1 with the corresponding ones calculated with MacroModel, shows that the solvent effect may substantially reduce the energy difference between the two conformers (see Table 1). These results further justify the selection of conformers used in CoMFA.

Despite the fact that, as expected, the 26 protonated compounds optimized by MacroModel showed a different charge distribution compared to those optimized by AM1, a CoMFA study performed on the former produced results (not shown) comparable to those reported in Table 3. Also in this case, better statistics were obtained when both steric and electrostatic fields were used.

For the molecular overlay two different strategies were envisaged. In a first series of superimpositions of charged (C) and neutral (N) I_2R ligands the following elements were used for the rigid fit on the corresponding atoms of the template **30** (alignments COa, NOa and CIa and NIa in Tables 2 and 3, respectively): (1) all the imidazoline heavy atoms; (2) the two heavy atoms in the bridge and all the aromatic carbons for compounds **1–22** and **35–38**; a similar criterion was adopted for the overlay of the bicyclic derivatives **23–28**; (3) the heavy atom in the bridge and the first aromatic carbon linked to it for compounds **39** and **40**; (4) the carbon atom in the bridge and the aromatic carbons 2′, 1′, 8′a, 8′ for compound **34**; and (5) the carbon atoms of the aromatic ring linked to imidazoline for compounds **29** and **31–33**.

Within the congeneric series of OPS also the diverse *ortho* substituents were superposed choosing the highly active cirazoline **3** as the 'inner' template.

In a second series of superimpositions few pharmacophoric elements were employed allowing more molecular flexibility in the fitting of both charged (C) and neutral (N) I_2R ligands. The following elements (alignments b) were adopted for the rigid fit on the corresponding atoms of the template: (1) the two

Table 3. Statistical results of CoMFA analysis of I_2R ligands **1–40**[a]

Alignment	q^2	ONC	n	r^2	s	F	Field(s)	Rel. contr.[b]
CI1a	0.379	4	40				ste	
CI2a	0.535	4	40				ele	
CI3a	0.640	4	40	0.893	0.405	73.56	ste + ele	53% ste; 47% ele
	0.661	5						
CI4b	0.351	4	40				ste	
CI5b	−0.028	1	40				ele	
CI6b	0.475	5	40	0.892	0.413	56.23	ste + ele	63% ste; 37% ele
NI1a	0.431	4	40				ste	
NI2a	0.203	2	40				ele	
NI3a	0.463	4	40	0.853	0.476	50.67	ste + ele	44% ste; 56% ele
	0.456	5						
NI4b	0.434	4	40				ste	
NI5b	0.566	4	40				ele	
NI6b	0.620	4	40	0.925	0.356	107.34	ste + ele	40% ste; 60% ele
	0.659	5						

[a]CI, NI: charged and neutral I_2R ligands, respectively; a and b: different alignment criteria (see text); q, ONC, n, r, s, F, and Field: see legend a of Table 2.
[b]Rel. contr.: relative contribution of steric and electrostatic CoMFA fields.

nitrogen atoms of the imidazoline ring and all the heavy atoms in the bridge; (2) the centroid of ring B of the bi- and tricyclic aromatic congeners (**29**, and **31–33**); and (3) the centroid of ring A of OPS ligands and of compounds **17–28**.

The *S* absolute configuration was chosen for idazoxan **23** and strictly related bicyclic congeners. Analogously, the same configuration was assigned to compounds **5**, **9**, **11**, and **14** bearing a chiral center on the oxymethylene bridge in a position corresponding to the chiral center of idazoxan.

The selection of the binding conformation of idazoxan **23** and related congeners deserves a particular comment.

Recent semi-empirical calculations by AM1 and PM3 Hamiltonians on both neutral and N_3-protonated forms of idazoxan,[24] showed the importance of the electrostatic interactions, probably a hydrogen bond, in determining the axial preference of the imidazoline ring in the minimum energy conformer which in the cation is more stable than the equatorial conformer by about 3.6 kcal/mol (AM1) or 2.6 kcal/mol (PM3). These results are in agreement with the crystallographic data on *S*-(+)-idazoxan hydrochloride single crystal.[19] The energy difference between axial and equatorial minimum energy conformers in the neutral molecule was instead very low, that is 0.55 and 0.66 kcal/mol from AM1 and PM3 calculations, respectively. However, according to the criterion of maximizing the overlap between the putative pharmacophoric points, in particular the key imidazoline ring atoms, a conformer very close to the global minimum of the equatorial form of protonated and neutral *S*-idazoxan was chosen for the fitting to the template. Only in this way was a good fit obtained: RMS = 0.23 and 0.38 Å for the equatorial conformer of charged and neutral ligands respectively, compared to RMS=1.08 and 1.26 Å for the corresponding axial conformers. A high molecular similarity, partly justifying the high I_2R affinity of idazoxan, may be seen only in the overlay of equatorial conformers. Similar conformations have been chosen for compounds **24** and **27** structurally related to idazoxan.

Table 4. Statistical results of CoMFA analysis of α_2-adrenoceptor ligands[a]

Alignment	q^2	ONC	n	r^2	s	F	Field(s)	Rel. contr.
CA1a	0.671	4	26	0.929	0.316	68.57	ste	
CA2a	0.553	4	26				ele	
CA3a	0.711	4	26	0.958	0.244	119.04	ste + ele	56% ste; 44% ele
CA4b	0.647	4	26	0.917	0.342	57.82	ste	
CA5b	0.495	4	26				ele	
CA6b	0.695	4	26	0.956	0.250	114.15	ste + ele	58% ste; 42% ele
NA1a	0.656	4	26	0.891	0.384	59.70	ste	
NA2a	0.532	2	26				ele	
NA3a	0.621	3	26	0.903	0.360	68.55	ste + ele	45% ste; 55% ele
NA4b	0.663	3	26	0.891	0.383	59.90	ste	
NA5b	0.545	2	26				ele	
NA6b	0.631	3	26	0.905	0.357	70.13	ste + ele	43% ste; 57% ele

[a]CA, NA: charged and neutral α_2-adrenoceptor ligands, respectively. See legend of Table 2 for the definition of symbols and abbreviations.

All the ligands were superimposed by the RIGIDFIT option of SYBYL (poorer results always came from the FIELDFIT option) and subjected to PLS analyses in conjunction with cross-validation (CV; leave-one-out method) to obtain the optimal number of components (ONC) to be used in the subsequent analyses. The PLS run was repeated with the ONC (see below) and a number of CV groups set to zero.

However, in strictly following this procedure there was a risk of obtaining overfitted models due to a relatively high value of components used. We therefore chose, from a plot of the cross-validated $r^2_{cv}(q^2)$ vs ONC, the first maximum in the curve which generally tended to reach a plateau. Those values are however reported on Tables 2–4 under the heading ONC.

This selection of a number of components lower than the ONC given by default in SYBYL yielded poorer statistics in terms of r^2 and standard deviations (worse fitting), but more realistic and trustworthy models.

PLS and CV permit the establishment of the optimal dimensionality of each model and thereby the derivation of the calibration equation with latent variables, which can be converted to the original parametric space represented by probe–ligand interaction energies. A 3-D QSAR equation is then produced and its coefficients, multiplied by the standard deviations associated to the energy variables, can be used to build the coefficient isocontour maps, which yield a meaningful pictorial representation of CoMFA results (see Figs 5, 6, 7, 11, and 12).

The statistical results obtained with the different alignments tested on charged and neutral I_2R ligands are shown in Tables 2 and 3 for the OPS and the whole set of imidazoline ligands, respectively. Results from separated and combined electrostatic and steric fields have also been listed.

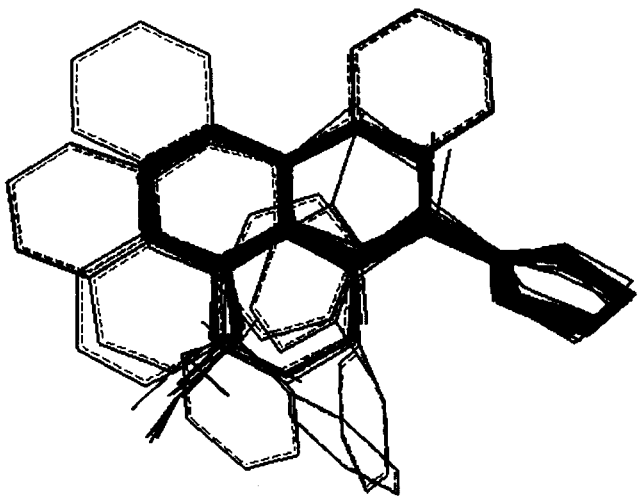

Figure 2. Overlay of I_2R ligands **1–40** according to alignment CI3a. The hydrogen atoms are omitted for clarity. The template **30** is represented as a bold line.

Tables 2 and 3 show statistically significant models in terms of predictive (q^2) and fitting (r^2 and s) power. In this regard, it can be observed that all the retained final CoMFA models had a q^2 value well above 0.30, which corresponds to a low probability of chance correlation ($p<0.05$, that is <5%).[25]

However, to be safer on the potential risk of chance correlations, the biological data were reassigned randomly to the compounds and the PLS analyses were repeated. In no case were good predictive models obtained (q^2 always <0.2).

The results reported in Tables 2 and 3 suggested that models from charged molecules presented better predictive ability (higher q^2) than the corresponding models of neutral molecules and, among them, alignment a yielded better results than alignment b. In addition, results in Table 3 show that the models combining steric and electrostatic fields yielded improved statistics both in terms of explained variance and predictive capability compared to models derived on a single field. However, in some instances, the ratio r^2/q^2 remains higher than desired and this may suggest some chance of overfitting related to the increased parametric dimensionality. Inasmuch as the analysis of the CoMFA contour maps revealed very specific features which help us to interpret the variations of data in a rational way, those models were retained.

In the case of the OPS congener (Table 2) models based on the steric field alone gave the best statistics. These findings were in full agreement with our 2-D QSAR study leading to equations 1 and 2.

The fitting power of the 3-D QSAR models giving the best statistics (alignments CO1a and CI3a; the latter is depicted in Fig. 2) may be seen on the plots of predicted vs observed pK_i reported in Figures 3 and 4,

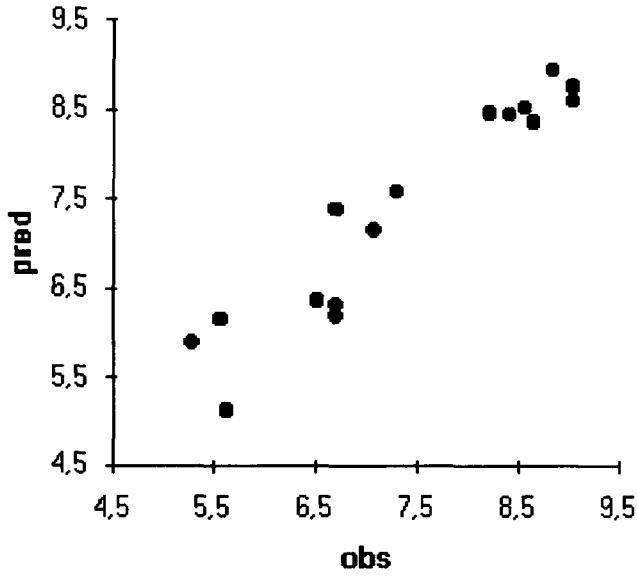

Figure 3. Plot of observed vs predicted pK_i values of OPS ligands **1–16**. Predicted pK_i are from noncross-validated equation CO3a.

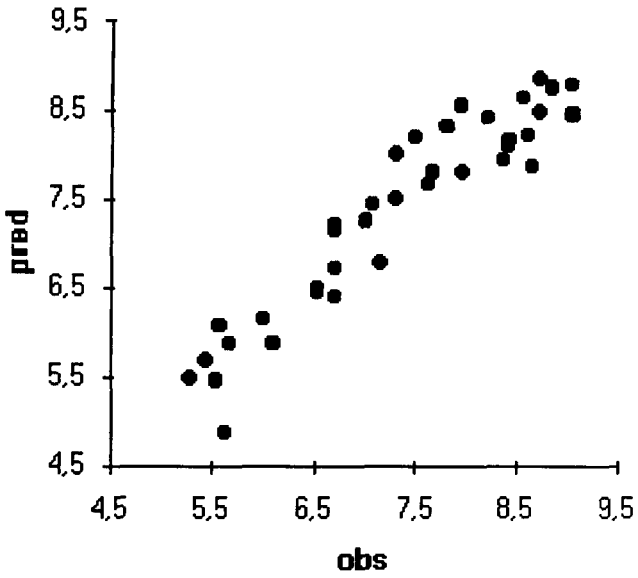

Figure 4. Plot of observed vs predicted pK_i values of I_2R ligands **1–40**. Predicted pK_i are from noncross-validated equation CI3a.

respectively. From the same models the CoMFA field-graph (isocontour maps) shown in Figures 5–7 were developed. Interestingly, only one compound, the benzylamino derivative **19**, was a strong outlier in model CI3a, displaying a residual value ($pK_{iobs} - pK_{ipred}$) about twice as high as the standard deviation *s*. A possible explanation for this strong deviation might be found in the peculiar structural nature of this derivative that is the only one presenting a basic center on the bridge.

The steric field graph for the OPS subset (Fig. 5) could be readily compared with equation 2. Unfavorable steric interactions were detectable mainly in the region occupied by the methyl substituents of the oxymethylene bridge (red zones), whereas the occupation of the green zone by small *ortho*-substituents increases the affinity. Bulky substituents could reach other (less evident) unfavorable steric regions represented by small red areas close to the allowed green zone.

Due to the intrinsic limitations of the data set composition of OPS, interactions of a different nature cannot be excluded. We have already planned the synthesis and testing of a new series of ligands bearing properly designed aromatic substituents, aiming at a better definition of the nature of receptor–ligand interactions in the space surrounding the phenoxy ring.

A close examination of the steric and electrostatic contour maps of I_2R ligands (Figs 6 and 7) revealed that the most important features observed in the model of OPS were conserved also in the global model and moreover further structural requirements for a strong receptor binding could be perceived.

The steric contour map (Fig. 6) revealed two large unfavorable regions (shown in red) where the methyl groups on the oxymethylene bridge, one chlorine atom of clonidine and some aromatic rings, may be positioned. A similar region, more limited in size, may be seen in the proximity of the other chlorine atom of clonidine and of the aromatic ring of the benzyl derivative **2**. One green zone, indicative of favorable steric interactions, may be also detected close to the small sized *ortho* substituents of OPS.

The electrostatic map (Fig. 7) showed one zone (cyan colored), partly occupied by the aromatic rings of the template and by the oxygen or sulfur atom of idazoxan and its congeners, where the increase of negative charge enhances the activity. Two yellow regions, where the increase of negative charge diminishes the activity, may be reached by the carbonyl group of the 4-chromenone derivative **28** by the π electron cloud of one phenyl group of the benzydryl congener **22** and possibly by methyl substituents on the bridge.

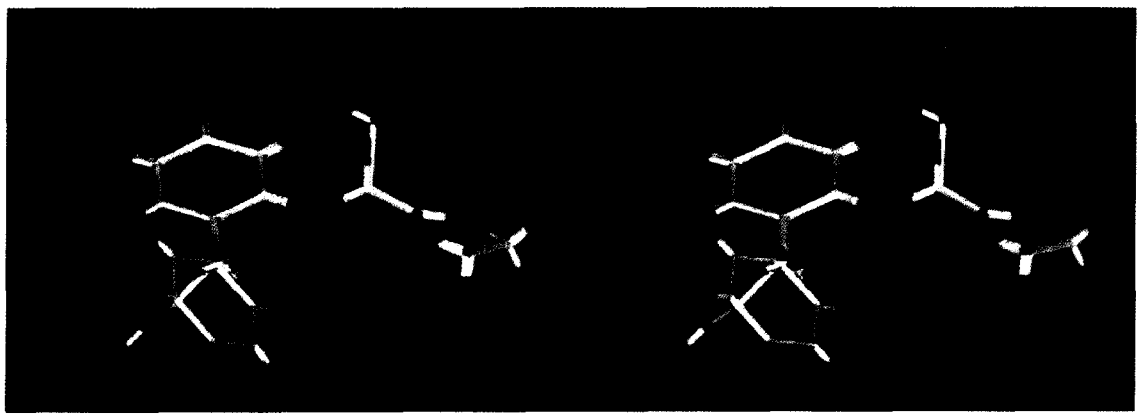

Figure 5. Stereoview of the steric STDEVxCOEFF contour plot for OPS model CO3a. Green and red regions indicated sterically favorable and unfavorable regions. respectively. The contour level is as follow: −0.170 red; 0.055 green. To aid interpretation OPS ligands **1**, **9**, and **12** are displayed.

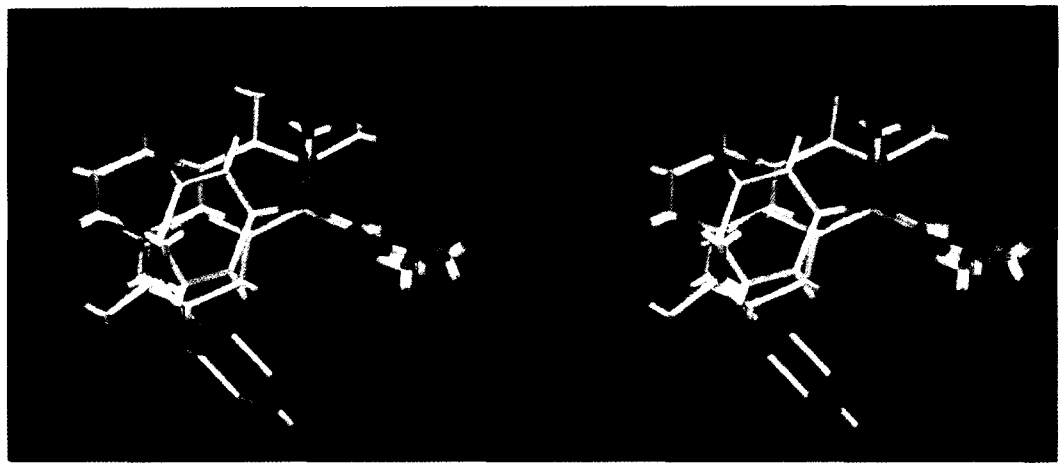

Figure 6. Stereoview of the CoMFA steric STDEVxCOEFF contour plot for I_2R model CI3a. The color for the steric field is as in Figure 5. The contour level is as follows: −0.080 red, 0.055 green; Compounds **2**, **4**, **14**, **31**, and **40** are displayed to aid interpretation.

α_2-Adrenoceptor binding affinities

Aiming at the determination of structural features responsible for I_2/α_2 receptor selectivity we also determined the α_2-adrenoceptor affinities for a large number of IR ligands (26 compounds) and extended our CoMFA study to this data set. Many additional affinity data have been published for a huge number of α_2-adrenoceptor ligands[26] but we preferred to restrict the analysis to our data set to avoid a dangerous mixing of data coming from different laboratories and experimental procedures. Our goal therefore was not the development of a comprehensive model for α_2-adrenoceptor ligands, but rather the formulation of a working hypothesis through the derivation of a 3-D QSAR model able to detect the main structural requirements for high α_2-adrenoceptor affinity and possibly for α_2/I_2R selectivity. For this reason neither the antagonist/agonist pharmacological profile nor any possible α_2-subtype selectivity (α_{2A} vs α_{2B} vs α_{2D})[27] were studied.

Our modeling studies, both on α_2 and I_2R ligands, were therefore based on the hypothesis that agonists and antagonists bind in a similar manner to the same receptor pocket. Even if no definite indications on the validity of this assumption are available, that has been a starting point for most modeling studies on ligands of G-protein coupled receptors.[28]

Like several other comparative modeling approaches,[29,30] the CoMFA methodology is also based on the assumption that similar molecules bind in a similar way to the same binding sites. Unfortunately, this is not always the case since it has been shown that even small structural variations may induce a completely different binding mode.[31] At the moment, this is a particularly strong limitation that has to be kept in mind, to avoid an erroneous overemphasization of the results from comparative modeling studies.

Very recently a molecular mechanics and quantum chemical study[9] on a limited number of α_2-adrenoceptor ligands (six compounds) led to a model that, it was claimed, explains the observed agonist and antagonist

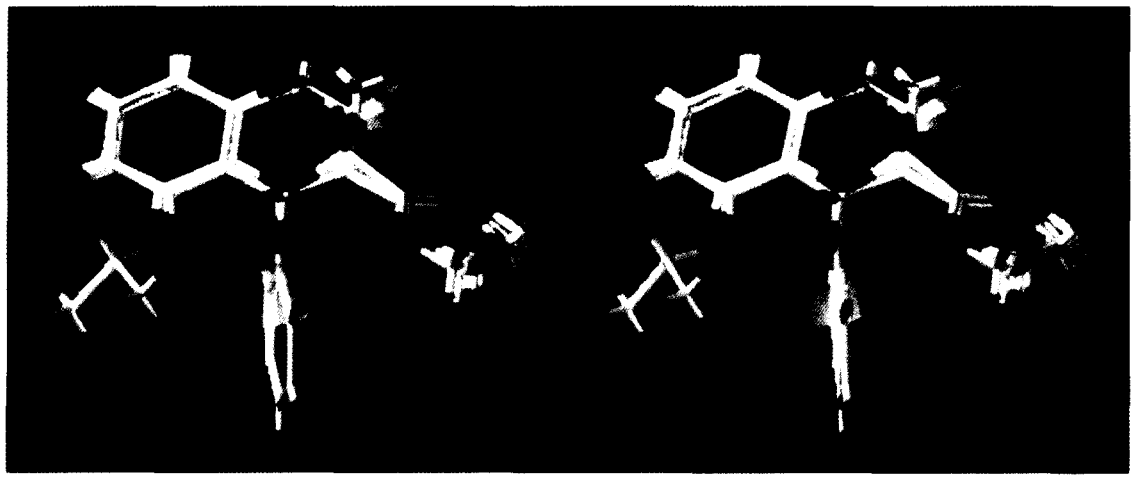

Figure 7. Stereoview of the CoMFA electrostatic STDEVxCOEFF contour plot for I_2R model CI3a. Favorable and unfavorable influences of high electron density are referred to as cyan and yellow regions, respectively. The contour level is as follows: −0.13 cyan, 0.17 yellow. The template **30**, compounds **11**, **22**, **23**, and **28** are displayed to aid interpretation.

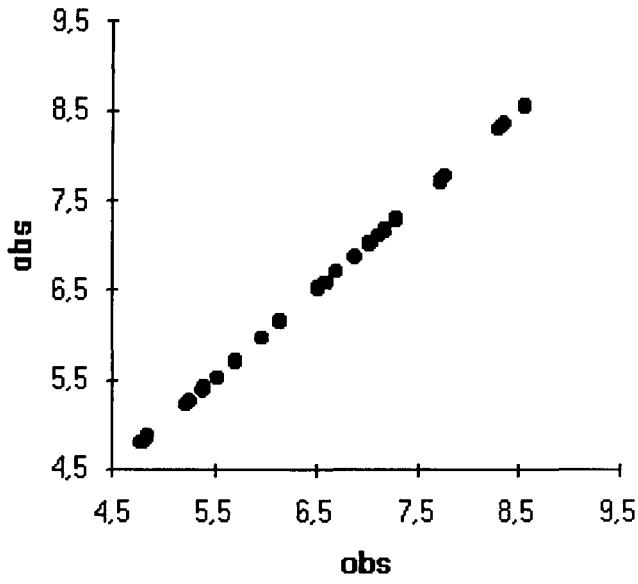

Figure 8. pK_i data distribution of α_2-adrenoceptor ligands.

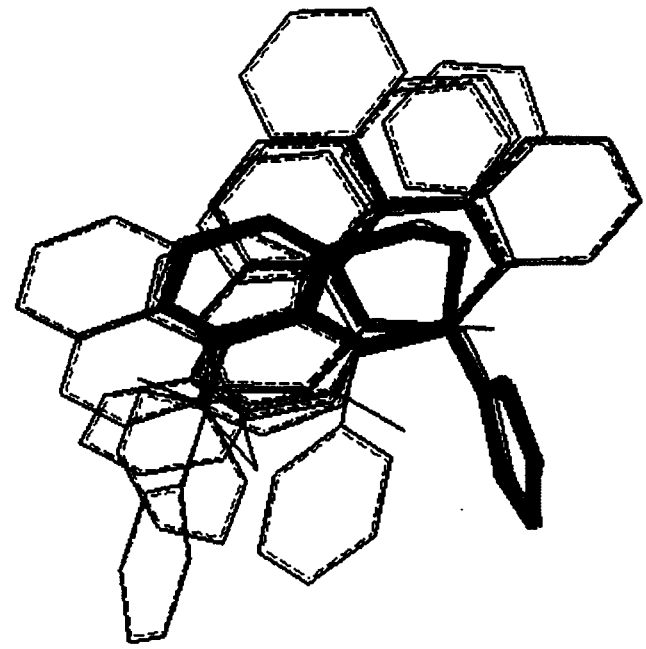

Figure 9. Overlay of α_2-adrenoceptor ligands according to alignment CA3a. The hydrogen atoms are omitted for clarity. The template **23** is represented as a bold line.

pharmacological profile on the basis of small structural changes.

In contrast with our approach, in that study a diverse alignment criterion based only on low energy conformations was used. Of course, this led to a model diverse from the one proposed by Carpy,[20] which was strictly based on X-ray-determined 3-D structures, and from ours (see below) especially in terms of the spatial location of the putative imidazoline ring.

Our models were derived from the analysis of a higher number of ligands (26 compounds) displaying α_2-adrenoceptor affinity data that are well distributed and span quite a wide range of about 4 log units (see Fig. 8).

For the molecular superpositions, the same alignment criteria used in the modeling of I_2R affinity were used. *S*-idazoxan, being a highly active (*S*-idazoxan showed a α_2-binding affinity much higher than its *R* enantiomer[32]) and rigid ligand, was selected as the template.

Unlike the I_2R ligands, there were no reasons to choose the less stable equatorial conformer, and therefore the axial minimum energy conformer related to N_3-protonated and neutral idazoxan was selected for the fitting of neutral and charged molecules according to alignments a and b already discussed. It is worth noting that a different dihedral angle ($OCCN_3 = 107.8°$ and $OCCN_3 = -127.7°$) corresponded to the protonated and neutral molecules, respectively.

Statistical results of CoMFA studies of both charged (CA) and neutral (NA) molecules are reported for alignments a and b in Table 4.

As in I_2R study, 3-D QSAR models of α_2 ligands, based on charged molecules and on alignments a, yielded the best statistical results although the differences with the models derived from neutral molecules were less pronounced. Moreover, the use of combined fields improved the statistics, with respect to single-field models, to a small but significant extent only in the case of protonated ligands.

However, in order to have a straightforward comparison with the 3-D QSAR models of I_2R ligands, alignment CA3a (depicted in Fig. 9) was chosen to develop a final 3-D QSAR model whose fitting capability may be judged from the plot shown in Figure 10. Figures 11 and 12 show the contribution of steric and electrostatic fields to CoMFA models.

The steric contour map (Fig. 11) suggests unfavorable steric interactions in two red colored regions, which can be reached by the aromatic rings of the anthryl (**31**) and phenanthryl (**32**) congeners. Favorable steric interactions may take place on the green colored region in which one chlorine atom of clonidine, and several aromatic rings of active ligands **23** and **24** may be positioned.

The electrostatic contour map depicted on Figure 12, shows two main areas, cyan and yellow colored, in which the increase of negative charge increases or decreases the binding affinity, respectively. The cyan region may be occupied by an aromatic ring of the most active ligand **34** and partly by one chlorine atom of clonidine **40**, one oxygen atom of idazoxan **23** and its strictly related congeners **24** and **25**.

The field graphs in Figures 11 and 12, are therefore able to satisfactorily explain at the 3-D level, the main

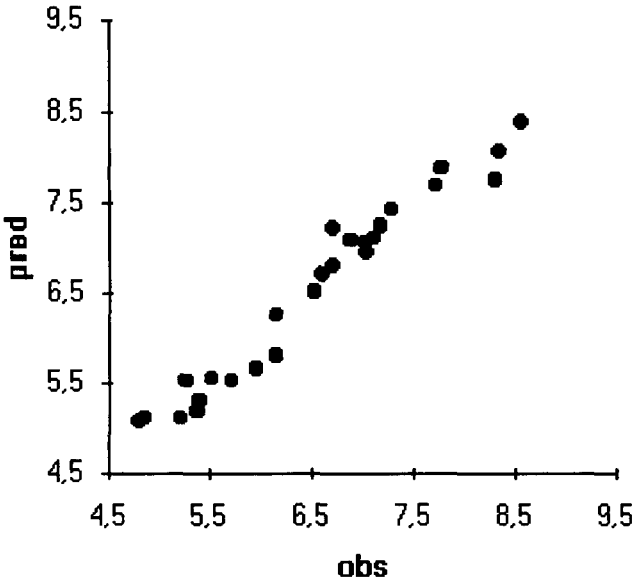

Figure 10. Plot of observed vs predicted pK_i values of α_2-adrenoceptor ligands **2–4**, **8**, **12–14**, **17**, **18**, **20**, **22–25**, **29–37**, **39**, and **40**. Predicted pK_i are from noncross-validated equation CA3a.

aspects of the structure–affinity relationship of α_2-adrenoceptor ligands.

I_2/α_2 receptor selectivity

The present study is a classic example where the observed receptor selectivity is due to the fact that the same compound may assume completely different conformations in the interaction with different receptors.

Actually, we have implicitly based our modeling studies of imidazoline and α_2-adrenoceptor binding affinities, on the hypothesis that two different binding modes may take place in the formation of the receptor–ligand complexes. In fact, our objectively correct choice of two different rigid templates (**30** and idazoxan **23** in the axial form), which presented a quite diverse orientation of the key imidazoline ring, played a determinant role for the development of CoMFA models with different 3-D features.

In other words, the relative orientation of the imidazoline and the hydrophobic moieties of the ligands was determined by the original selection of the templates, which, however, was based on experimentally irrefutable evidence of a high activity associated to rigid molecules.

Keeping in mind the above observations, some structural requirement for I_2/α_2 receptor selectivity may be perceived comparing the spatial orientations of the ligands showing the highest and the lowest selectivity. In doing so, we restricted our selection to seven compounds, four presenting a tighter binding to I_2R (**30**, **17**, **20**, and **33**) and three that conversely showed a tighter binding to α_2-adrenoceptor (**40**, **14** and **34**). It is worth stressing that all the ligands with the highest selectivity for I_2R may assume a more or less planar conformation, with the imidazoline ring slightly out of plane as shown by a mean value of $-35.5°$ for the dihedral angle ϕ.

On the other hand, compounds with the greatest selectivity toward the α_2-adrenoceptor, may assume a more distorted (puckered) conformation leading to a mean dihedral angle $O(C)CCN_3$ of 106.2°, a value completely different from the one observed for selective I_2R ligands. These two different binding modes for selective I_2 and α_2 receptor ligands may be more clearly seen in the molecular overlays reported in Figure 13. I_2R selective ligand conformations in Figure 13 came from alignment CI3a, whereas α_2 selective ligand conformations were from alignment CA3a. Analogously to the alignment criteria a and b previously used for the

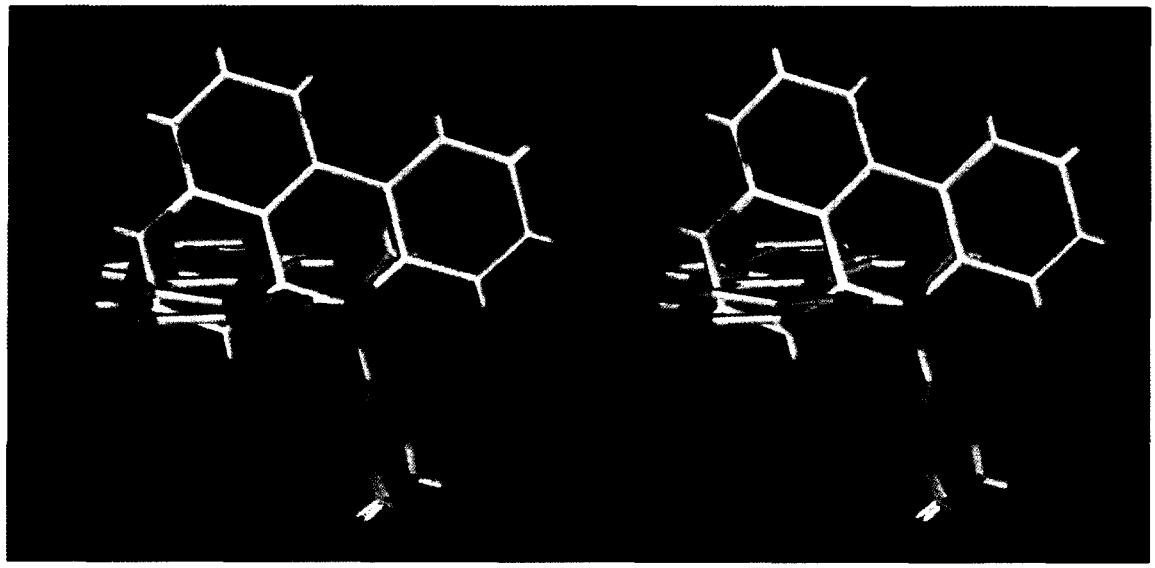

Figure 11. Stereoview of the CoMFA steric STDEVxCOEFF contour plot for α_2 model CA3a. The color code is as in Figure 5. The contour level is as follows: −0.042 red, 0.060 green. The template **23** and compounds **31**, **32**, **34**, and **40** are displayed to aid interpretation.

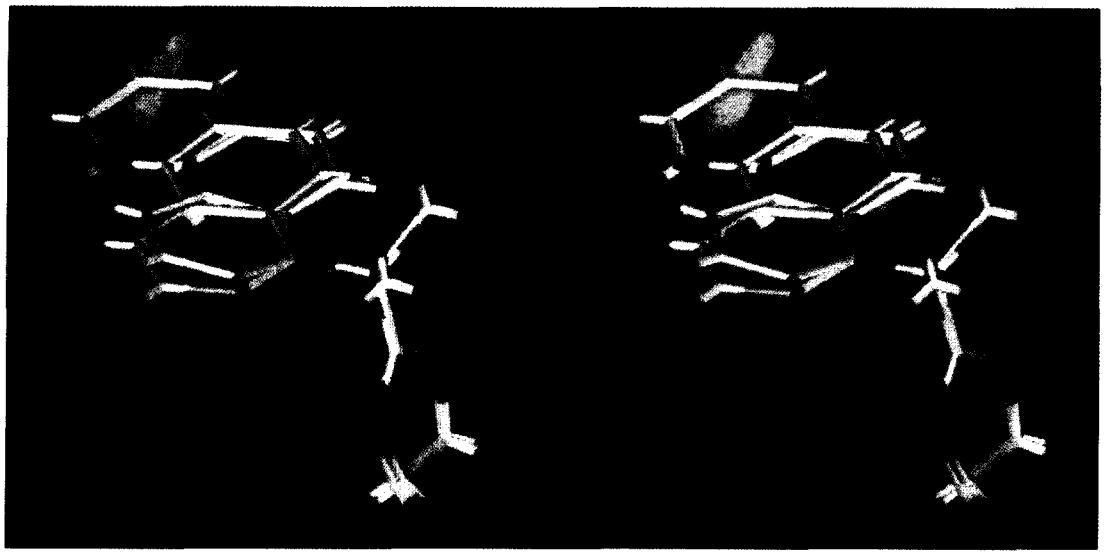

Figure 12. Stereoview of the CoMFA electrostatic STDEVxCOEFF contour plot for α_2 model CA3a. The color code is as in Figure 7. The contour level is as follows: −0.10 cyan, 0.082 yellow. The template **23** and compounds **34**, **38**, and **40** are displayed to aid interpretation.

development of CoMFA 3-D models, two different overlays c and d were made as reported on the left and right-hand sides, respectively (Fig. 13). In alignment c, only the heavy atoms of the imidazoline ring were fitted whereas in alignment d, the two nitrogen atoms and the centroid defined by the benzene ring and the heavy atoms in the bridge were used for fitting.

The two diverse alignments may refer to two possibly different binding modes: one which is exclusively driven by the electrostatic interactions (charge reinforced hydrogen bond?) of the imidazoline ring and one in which the electrostatic interactions of the same ring are counterbalanced by possible hydrophobic (or π–π stacking) interactions, involving the aromatic rings.

In the former case, once the electrostatic interactions, most likely with the carboxyl group of an aspartic acid, have been set out the selectivity may arise from a differently located hydrophobic region in the binding site of the two receptors. In the other case, while it is still possible that a different position of the hydrophobic regions might also contribute to the overall selectivity, this may also be caused by a different location of the carboxylic acid group on the two receptors.

Since quite diverse initial conformations were used to develop the 3-D QSAR models for I_2 and α_2 receptor ligands, an overall different spatial disposition of the putative electrostatic and steric regions determining the variation of the binding affinity had to be expected. Indeed this can be immediately perceived by a visual, albeit approximative, comparison of the putative characteristics of the electrostatic and steric contour maps of the two receptor ligands (Figs 6 and 7 vs Figs 11 and 12).

The most evident differences in the steric maps reside in: (1) the stronger negative steric effect of the C-CH_3 substituent (red region) on the I_2 than on the α_2 affinity. (2) The opposite effect exerted by one clonidine chlorine atom, sterically favorable on the α_2 (green region), unfavorable on the I_2 receptor (red region). (3) The opposite effect of some aromatic ring as in the case of 2′-naphthyl **30** and styryl **20** derivatives.

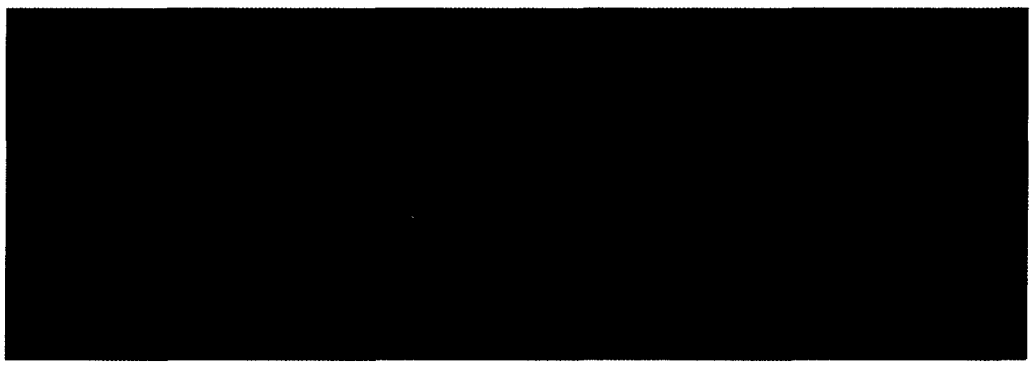

Figure 13. Molecular superimposition of I_2 and α_2 selective receptor ligands (red and green colored, respectively) according to alignment c (right-hand side) and d (left-hand side).

In the comparison of the electrostatic contour maps, the chlorine atom of clonidine exerts, once again, an opposite electrostatic effect occupying a cyan and yellow region on the α_2 and I_2 maps, respectively.

A similar effect may be seen for congeners **29–32**, which placed some aromatic ring on a cyan or yellow region in the α_2 and I_2 ligand field graphs.

Conclusions

Congruent 2-D and 3-D QSAR analyses allowed us to gain important insight into the key structural features governing the binding of a large series of I_2R ligands. Similarly, 3-D QSAR study of the α_2-adrenoceptor binding affinity showed some peculiar electrostatic and steric properties, which favored a strong receptor binding.

A comparison of the possible bound conformations of I_2 and α_2 receptor ligands, as well as of their steric and electrostatic 3-D isocontour maps, suggested likely structural requirements for receptor selectivity. In particular, more planar ligand conformations seem to characterize the binding to I_2R, whereas more puckered conformations seem to be involved in the binding to α_2-adrenoceptor. In addition, a different location of a large hydrophobic region, and possibly of a carboxylic group, in the two receptors may be determinant topological features for I_2/α_2 selectivity.

The synthesis of properly designed 2-substituted imidazolines having different degree of conformational freedom and carrying proper substituents in particular positions is underway with the aim of improving and refining our 3-D models for binding and selectivity.

Experimental

2-D QSAR study

Cross-validated multilinear regression was carried out with the 'c-QSAR' software (Biobyte Corp., Claremont, CA, USA).[33]

Verloop STERIMOL parameters (L_1, B_1 and B_5), Charton steric parameters (v) and molar refractivity (MR) were taken from standard compilations.[11,34]

Molecular modeling and CoMFA study

Molecular models of the neutral and N_3-protonated I_2R ligands **1–40** were constructed with standard bond distances and angles using SYBYL (v. 6.2) software (Tripos Assoc. St Louis, MO, USA) running on a Silicon Graphics Indigo2 R4400 workstation. The option CRYSIN was used for building *S*-(+)-idazoxan and clonidine, starting from their X-ray crystallographic data. Full geometry optimization was performed with the AM1 Hamiltonian using the parameter set reported in the MOPAC (v. 6.0) suite of programs.[35] The partial Mulliken atomic charges from AM1 calculations were used in the CoMFA study.

The conformational analysis was carried out with the SYSTEMATIC SEARCH option of SYBYL, screening the conformational space of each torsion angle at 30° increments.

It is worth noting that, in agreement with literature data,[19] the N_3-protonated imidazoline ring is symmetric and this facilitated the conformational search by halving the number of possible rotamers.

All the generated conformers were optimized by the Tripos standard Force Field (MAXIMIN2)[36] and those retained for the subsequent fit and CoMFA analysis (see text) were re-optimized by AM1. The molecular superimpositions for CoMFA were made with the RIGIDFIT option of SYBYL. The different alignment criteria chosen to test diverse spatial orientations of the ligands, have already been discussed. The RMS (root mean squares) value of the fitted points was used to assess the quality of the fit.

Conformational analysis and geometry optimization were also performed (see text) by the *solvent continuum* method and the AMBER* Force Field as implemented in the molecular modeling software MacroModel (v. 5, C. Still, Columbia University, New York, NY, USA)

The CoMFA study was carried out using the QSAR module of SYBYL. Default settings were used in the analyses, except for the 'drop-electrostatic' option, which was set to 'no'. The steric and electrostatic interaction energies were calculated on grid points of a regularly spaced 3-D lattice with an sp^3 carbon probe atom having a charge of +1 and a van der Waals radius of 1.52 Å. The grid size had a resolution of 2 Å and the region dimensions were defined with the 'molecular volume' automatic mode.

CoMFA was performed in two successive steps. In a first analysis, using eight components and a number of cross-validation groups equal to the number of compounds, the optimal number of components (ONC) was determined. The ONC is that number of components which yielded the highest cross-validated r^2_{cv} (q^2) values which is defined as $q^2 = (SD - PRESS)/SD$, where SD is the sum of squares of deviations of the observed values from their mean and PRESS is the prediction error sum of squares.

In the second step, the analysis was repeated without cross-validation using the ONC previously determined (see text). The results of the last analysis were used to produce the final 3-D QSAR models from which the coefficient isocontour maps depicted in Figures 5, 6, 7, 11 and 12 were drawn.

The predictive and fitting capabilities of the models were measured by the cross-validated r^2 (q^2) and r^2 (and s, standard deviation), respectively.

Acknowledgments

The financial support of CNR (Rome) and MURST (40% funds, Rome) is gratefully acknowledged.

References

1. Cramer, R. D.; Patterson, D. E.; Bunce, J. D. *J. Am. Chem. Soc.* **1988**, *110*, 5959.

2. Cramer, R. D.; De Prierst, S. A.; Patterson, D. E.; Hect, P. In *3D QSAR in Drug Design: Theory, Methods and Applications*; Kubinyi, H., Ed.; Escom: Leiden, 1993; pp 443–485.

3. Dunn, III, W. J.; Wold, S.; Edlund, U.; Helberg, S. *Quant. Struct.-Act. Relat.* **1984**, *3*, 131.

4. Wold, S.; Johansson, E.; Cocchi, M. In *3D QSAR in Drug Design: Theory, Methods and Applications*; Kubinyi, H., Ed.; Escom: Leiden, 1993; pp 523–549.

5. Cramer, R. D.; Bunce, J. D.; Patterson, D. E. *Quant. Struct.-Act. Relat.* **1988**, *7*, 18.

6. Pigini, M.; Bousquet, P.; Carotti, A.; Dontewill, M.; Giannella, M.; Moriconi, R.; Piergentili, A.; Quaglia, W.; Tayebati, K. S.; Brasili, L. *Bioorg. Med. Chem.*, this issue.

7. Trumpp-Kallmeyer, S.; Hoflack, J.; Bruinvels, A.; Hibert, M. *J. Med. Chem.* **1992**, *35*, 3448.

8. Ruffolo, Jr, R. R.; Nichols, A. J.; Stadel, J. M.; Hieble, J. T. *Pharmacol. Rev.* **1991**, *43*, 475.

9. Rouvinen, J.; Hoffren, A.; Karjalainen, A.; Tapani, A. P. *Drug Des. Disc.* **1993**, *10*, 285.

10. Kubinyi, H. *QSAR: Hansch Analysis and Related Approaches*; VHC; Weinheim, 1993.

11. Hansch, C.; Leo, A.; Hoeckman, D. *Exploring QSAR*; ACS:Washington, 1995; Vols 1 and 2.

12. Kneubühler, S.; Thull, U.; Altomare, C.; Carta, V.; Gaillard, P.; Carrupt, P.-A.; Carotti, A.; Testa, B. *J. Med. Chem.* **1995**, *38*, 3874.

13. Carrieri, A.; Altomare, C.; Barreca, M. L.; Contento, A.; Carotti, A.; Hansch, C. *Il Farmaco* **1994**, *49*, 573.

14. Carotti, A.; Raguseo, C.; Campagna, F.; Langridge, R.; Klein, T. E. *Quant. Struct.-Act. Rel.* **1989**, *8*, 1.

15. Altomare, C.; Carotti, A.; Cellamare, S.; Carrupt, P.-A.; Testa, B. *Chirality* **1993**, *5*, 527.

16. Carotti, A.; Altomare, C.; Cellamare, S.; Monforte, A. M.; Bettoni, G.; Loiodice, F.; Tangari, N.; Tortorella, V. *J. Comp.-Aided Mol. Des.* **1995**, *9*, 131.

17. Hansch, C.; Leo, A. In *Substituent Constants for Correlation Analysis in Chemistry and Biology*; John Wiley: New York, 1979.

18. Selassie, C. D.; Klein, T. E. In *3D QSAR in Drug Design: Theory, Methods and Applications*; Kubinyi, H., Ed.; Escom: Leiden, 1993; pp 257–275.

19. Cattier-Humblet, C.; Carpy, A. *Eur. J. Med. Chem.-Chim. Ther.* **1985**, *20*, 251.

20. Carpy, A.; Leger, J. M.; Leclerc, J.; Dacker, N.; Ruot, B.; Vermuth, C. G. *Mol. Pharmacol.* **1982**, *21*, 400.

21. Sung, J. C.; Tropsha, A. *J. Med. Chem.* **1995**, *38*, 1060.

22. Brasili, L.; Pigini, M.; Bousquet, P.; Carotti, A.; Dontenwill, M.; Giannella, M.; Moriconi, R.; Piergentili, A.; Quaglia, W.; Tayebati, K. S. In *Perspectives in Receptor Research*; Giardin, D.; Piergentili, A.; Pigini, M., Eds.; Elsevier: Amsterdam, 1996; pp 361–373.

23. Nicklaus, M. C.; Wang, S.; Driscole, J. S.; Milne, G. W. A. *Bioorg. Med. Chem.* **1995**, *4*, 411.

24. Hariharan, S.; Shelver, H. W. *Int. J. Quant. Chem.* **1992**, *44*, 181.

25. Agarwal, A.; Pearson, P. P.; Taylor, E. W.; Li, H. B.; Dahlgren, T.; Herslof, M.; Yang, Y.; Lambert, G.; Nelson, D. L.; Regan, J. W.; Martin, A. R. *J. Med. Chem.* **1993**, *36*, 4006.

26. Hieble, J. P.; Bondinell, W. E.; Ruffolo, Jr, R. R. *J. Med. Chem.* **1995**, *38*, 3415 and 3681

27. Bylund, D. B. *FASEB J.* **1992**, *6*, 832.

28. Hoflack, J.; Trumpp-Kallmeyer, S.; Hubert, M. In *3D QSAR in Drug Design: Theory, Methods and Applications*; Kubinyi, H., Ed.; Escom: Leiden, 1993; pp 355–373.

29. Thibaut, U. In *3D QSAR in Drug Design: Theory, Methods and Applications*; Kubinyi, H., Ed.; Escom: Leiden, 1993; pp 661–696.

30. Carotti, A.; Altomare, C. *La Chim. Ind.* **1995**, *77*, 13.

31. Mattos, C.; Ringe, D. In *3D QSAR in Drug Design: Theory, Methods and Applications*; Kubinyi, H., Ed.; Escom: Leiden, 1993; pp 226–254.

32. Dabir, H.; Mouille, P.; Schmitt, H. *Eur. J. Pharmacol.* **1983**, *86*, 83.

33. Hansch, C.; Leo, A. *QSAR Database*. Biobyte Corp.: Claremont, CA, U.S.A.

34. van de Waterbeemd, H.; Testa, B. In *Advances in Drug Research*; Testa, B.; Ed.; Academic: New York, 1987; Vol. 16, pp 85–225.

35. MOPAC 6.0 is available from QCPE (506).

36. Clark, M.; Cramer.; R. D. Van Opdenbasch, N. *J. Computat. Chem.* **1989**, *10*, 982.

37. Ferguson, D. M.; Kolman, P. A. ibid **1991**, *12*, 620; and references therein.

(*Received in U.S.A.* 1 *August* 1996; *accepted* 20 *January* 1997)